Dentomaxillofacial Radiology (2015) 44, 20140322

birpublications.org/dmfr

RESEARCH ARTICLE

Comparison of mandibular bone microarchitecture between micro-CT and CBCT images

[1]S Panmekiate, [1]N Ngonphloy, [1]T Charoenkarn, [1]T Faruangsaeng and [1,2]R Pauwels

[1]*Department of Radiology, Faculty of Dentistry, Chulalongkorn University, Bangkok, Thailand;* [2]*OMFS-IMPATH Research Group, Oral Imaging Center, Department of Imaging and Pathology, Faculty of Medicine, Catholic University of Leuven, Leuven, Belgium*

Objectives: To compare microarchitecture parameters of bone samples scanned using micro-CT (μCT) to those obtained by using CBCT.
Methods: A bone biopsy trephine bur (3 × 10 mm) was used to remove 20 cylindrical bone samples from 20 dry hemimandibles. Samples were scanned using μCT (μCT 35; SCANCO Medical, Brüttisellen, Switzerland) with a voxel size of 20 μm and CBCT (3D Accuitomo 170; J. Morita, Kyoto, Japan) with a voxel size of 80 μm. All corresponding sample scans were aligned and cropped. Image analysis was carried out using BoneJ, including the following parameters: skeleton analysis, bone surface per total volume (BS/TV), bone volume per total volume (BV/TV), connectivity density, anisotropy, trabecular thickness and spacing, structure model index, plateness and fractal dimension. Pearson and Spearman correlation coefficients (*R*) were calculated. CBCT values were then calibrated using the slope of the linear fit with the μCT values. The mean error after calibration was calculated and normalized to the standard deviation of the μCT values.
Results: *R*-values ranged between 0.05 (plateness) and 0.83 (BS/TV). Correlation was significant for both Spearman and Pearson's *R* for 8 out of 16 parameters. After calibration, the smallest normalized error was found for BV/TV (0.48). For other parameters, the error range was 0.58–2.10.
Conclusions: Despite the overall correlation, this study demonstrates the uncertainty associated with using bone microarchitecture parameters on CBCT images. Although clinically relevant parameter ranges are not available, the errors found in this study may be too high for some parameters to be considered for clinical application.
Dentomaxillofacial Radiology (2015) **44**, 20140322. doi: 10.1259/dmfr.20140322

Cite this article as: Panmekiate S, Ngonphloy N, Charoenkarn T, Faruangsaeng T, Pauwels R. Comparison of mandibular bone microarchitecture between micro-CT and CBCT images. *Dentomaxillofac Radiol* 2015; **44**: 20140322.

Keywords: cone-beam computed tomography; microcomputed tomography; bone; bone quality; computer-assisted image processing

Introduction

The success rate of oral implants has been proposed to pertain to bone quality, among other factors.[1–5] The concept of bone quality has recently evolved from a density-based approach towards a structural approach, as it has been shown that trabecular bone microarchitecture affects implant stability.[6] The pre-operative analysis of trabecular structure could therefore predict patient outcome and be used to select (un)favourable implant sites.

Conventional histomorphometry has been used as the gold standard for analysing bone microarchitecture,

Correspondence to: Dr Ruben Pauwels. E-mail: pauwelsruben@hotmail.com

Financial support was received from Faculty of Dentistry, Chulalongkorn University, Bangkok, Thailand.
Received 11 September 2014; revised 14 November 2014; accepted 6 January 2015

such as the percentage of bone tissue.[7] However, this method is irreversible, takes a long time and is costly. In addition, it provides just two dimensions of the three-dimensional specimen. Micro-CT (μCT) has been validated[8] and is presently implemented as the new gold standard method for quantifying bone microarchitecture.[9] Nevertheless, this method is limited to the investigation of small animal (*in vivo*) or biopsy (*ex vivo*) specimens and cannot be applied for clinical imaging.

Currently, CBCT systems have evolved to offer images with higher resolution than do early generation CBCTs.[10] High-resolution CBCTs use voxel sizes as small as 0.08 mm and are being used to visualize small anatomical details and pathologies in the oral region. This has raised the question whether CBCT images can be used to quantify trabecular microarchitecture on patient images. While it can be expected that CBCT and μCT images do not yield identical values for bone quality parameters because the latter has superior image sharpness, it might be possible to obtain stable bone microarchitecture measurements for CBCT images and to relate these values to clinical bone quality and thus, implant outcome or bone healing.

The aim of this study was to compare micro-architecture parameters of bone samples scanned using μCT to those obtained by using CBCT.

Methods and materials

The study protocol was approved by the human research ethics committee of the Faculty of Dentistry, Chulalongkorn University, Bangkok, Thailand (study code HREC-DCU-2013-058).

Sample preparation

20 cylindrical bone samples were removed from 20 cadaver hemimandibles that had edentulous ridges posterior to the mental foramen. A bone biopsy trephine bur (3 × 10 mm) was used for the removal. Samples were placed in Styrofoam holders (Dow Chemical Co., Midland, MI) for scanning by CBCT and μCT, in order to mimic the orientation of an implant site.

CBCT and micro-CT scanning

Samples were scanned using μCT (μCT 35; SCANCO Medical, Brüttisellen, Switzerland) with radiographic parameters of 70 kVp, 114 μA, 0.5-mm aluminium filter, 360° rotation, 450 basis projections and an isotropic voxel size of 20 μm. On the same day, samples were scanned by CBCT (3D Accuitomo 170; J. Morita, Kyoto, Japan) using a field of view of 4 × 4 cm, 90 kVp, 62 mAs, 2.5-mm aluminium filter, 360° rotation and 970 basis projections with an isotropic voxel size of 80 μm. For the CBCT, the mA used was 60% lower than that used for standard patients to avoid overexposure of the detector. Reconstructed images were exported as multifile image data and converted into single-file tag image files for analysis. Image analysis comprised four steps: alignment, cropping, thresholding and bone analysis (Figure 1).

Alignment of micro-CT and CBCT images

The samples were manually aligned in the coronal, sagittal and axial planes to ensure that the μCT and CBCT images were in the same orientation using ImageJ (US National Institutes of Health, Bethesda, MD). First, samples were aligned vertically in both the coronal and sagittal planes, ensuring that their long axis is parallel to these planes. For the axial plane, CBCT and μCT images were matched, that is, μCT images of each sample were rotated using the corresponding CBCT image as a visual template. Axial images after matching are shown in Figure 2. Alignment in all three planes was performed by two observers in order to minimize observer bias. When differences of >3° were found, the alignment was repeated until the deviation was <3°. The average rotation angles from the two observers, discarding angles differing >3°, were then selected for final alignment.

After alignment, all μCT and CBCT scans were tightly cropped to limit the amount of air space around

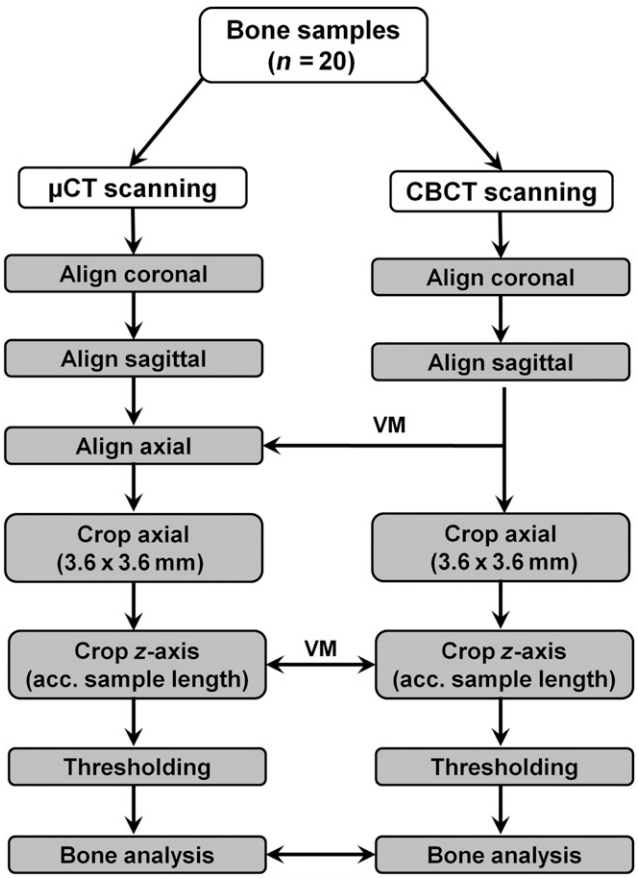

Figure 1 Workflow of image analysis. First, CBCT images were aligned along the *z*-axis by rotating the coronal and sagittal planes. Second, axial micro-CT (μCT) images were rotated using corresponding CBCT images as visual templates. Third, all images were cropped to 3.6 × 3.6 mm in the axial plane, and to corresponding sizes (according to the length of the bone sample) along the *z*-axis using visual matching (VM). Finally, all images were thresholded and underwent bone analysis.

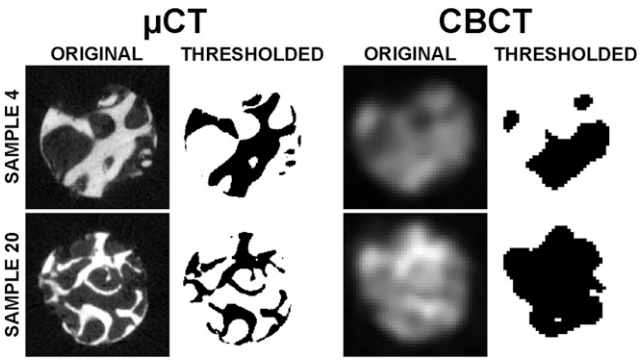

Figure 2 Original and automatically thresholded images from micro-CT (μCT) and CBCT, aligned in the axial plane.

the bone to a minimum. It was ensured that the total volume for each corresponding μCT and CBCT scans was identical. In the axial plane, this was carried out by manually cropping each image to a size of 3.6×3.6 mm (*i.e.* 180×180 voxels for μCT, 45×45 voxels for CBCT), ensuring that the cropped images fully encompassed the bone sample. In the coronal/sagittal planes (*i.e.* *z*-axis cropping) each sample was cropped according to its exact length, matching the cropped length for each corresponding CBCT and μCT image by use of the voxel size (*e.g.* 500 voxels for μCT, 125 voxels for CBCT = 10 mm in both images), and visually matching the start and end points of the cropped image.

Thresholding

To segment the bone from the images, they were thresholded and converted into a binary image (Figure 2). Various thresholding algorithms available in ImageJ were visually evaluated. The stack-based "Moments" method was selected, as it provided the most consistent bone segmentation.[11] Figure 3 shows a binary CBCT sample image at various manually set threshold values as a comparison; it can be seen that it was not possible to manually obtain a better segmentation than with the automatic thresholding shown in Figure 2.

Analysis of bone microarchitecture

Image analysis was carried out using ImageJ by means of the BoneJ plugin (http://www.bonej.org).[12] The following parameters were included:

- bone surface per total volume (BS/TV)[13]
- bone volume per total volume (BV/TV)
- fractal dimension[14]
- connectivity density[15,16]
- anisotropy[17,18]
- trabecular thickness (Tb.Th) and spacing (Tb.Sp)[19,20]
- structure model index (SMI);[21] both the overall SMI and its positive and negative components were calculated
- plateness, an alternative for SMI. Plateness is expressed as the ratio of eigenvalues (ev) along the longest (ev1), middle (ev2) and shortest (ev3) axis of the trabeculae
- skeleton analysis;[22] the following parameters associated with the skeletonized image of the samples were included: number of branches, number of junctions, branch length and triple points.

Analysis of results and statistics

Statistical analysis was performed using Prism 5.01 (GraphPad Software, San Diego, CA). Interobserver agreement was evaluated by comparing the angles used to align the samples. The originally determined angles, including those for which deviations between observers was >3°, were used for this comparison. Spearman correlation was used, as the data did not pass the D'Agostino and Pearson omnibus normality test ($p < 0.01$). In addition, the Wilcoxon signed rank test (*i.e.* a non-parametric paired test) was used at a significance level α of 0.05.

To correlate μCT to CBCT values for each parameter, Pearson (R_P) and Spearman (R_S) correlation coefficients were calculated, and *p*-values corresponding to a linear regression were determined, with $p < 0.05$ considered to be statistically significant. The rationale of using both Pearson's and Spearman's *R* is that the former corresponds to a linear fit, whereas the latter is valid for any monotonous relationship between two variables. While the former is conventionally used for normally distributed data and the latter as a non-parametric alternative, normality of the data was not relevant for in this study.

Figure 3 CBCT image of Sample 20 (also shown in Figure 2, bottom row) at various threshold values.

Paired *t*-tests, or Wilcoxon signed rank tests in case of non-normally distributed data, were performed on the μCT and CBCT values. $p < 0.05$ was considered as statistically significant.

Next, CBCT values were calibrated to the μCT values in order to estimate the applicability of calibration coefficients for each bone parameter. These calibration coefficients corresponded to the slope of a linear fit between the CBCT and μCT values, passing through ($x = 0$, $y = 0$), with the formula:

$$y = a \times x \quad (1)$$

with y the calibrated CBCT value, a the calibration coefficient and x the original CBCT value. The mean error after calibration (*i.e.* the average difference between calibrated CBCT value and μCT value for the 20 samples) was calculated for each bone parameter and normalized to the standard deviation of the μCT values for that particular parameter. This normalization was carried out in order to take the "normal spread" of the values into account, as some of the investigated parameters can have a wide range of values (*e.g.* BV/TV), whereas others are limited to a narrow range (*e.g.* fractal dimension).

Results

Correlation, expressed as R_S, between alignment angles used by the two observers was 0.56. Wilcoxon signed rank test revealed no significant difference between the angles ($p = 0.74$).

Correlation between CBCT and micro-CT

Table 1 shows correlation coefficients (R) for CBCT *vs* μCT values for all bone parameters. The highest R-value was seen for BV/TV ($R_P = 0.80$, $R_S = 0.73$) and BS/TV ($R_P = 0.67$, $R_S = 0.83$). Six other parameters showed a statistically significant correlation for both R_P and R_S ($p < 0.05$): branch length, anisotropy, Tb.Th, trabecular spacing, fractal dimension and the negative component of SMI. Connectivity density, SMI and positive SMI showed a significant Spearman but not Pearson correlation. Branches, junctions, triple points and the plateness parameters ev2/ev1 and ev3/ev1 showed no significant correlation. For BS/TV, Tb.Th and SMI, R_S was notably higher than R_P (+0.14 or more), which may indicate that a linear fit may not be the best option for these parameters; the applicability of different types of non-linear fits was not further explored in this study.

Figures 4–6 depict scatter plots with linear regression lines. Although several parameters show a notable correlation between μCT and CBCT values, several data points with large deviations can be spotted. Furthermore, in most cases, the linear fit does not traverse through (0, 0) making it somewhat unrealistic.

Calibration of CBCT values

Table 1 contains calibration coefficients used to convert CBCT values for error estimations. A calibration coefficient equal to 1 implies that, on average, the numerical values for CBCT and μCT corresponded exactly, a value >1 corresponds to CBCT underestimation relative to μCT and <1 to overestimation. CBCT showed severe underestimation for branches, junctions and connectivity density, and an underestimation by a factor

Table 1 Correlation coefficient, calibration coefficient and normalized error for each bone parameter

	R, *CBCT–μCT*			*Error normalized to SD of μCT values*	
Bone parameter	*Pearson*	*Spearman*	*Calibration coefficient*	*Mean*	*Max*
Skeleton analysis					
Branches	0.41	0.37	40.025	1.04	3.06
Junctions	0.42	0.35	37.062	1.04	3.42
Branch length	0.49[a]	0.52[a]	0.253	0.58	2.48
Triple points	0.40	0.33	34.755	1.10	3.70
BS and volume					
BS/TV	0.67[a]	0.83[a]	1.995	0.64	1.67
BV/TV	0.80[a]	0.73[a]	0.767	0.48	1.26
Trabecular structure					
Anisotropy	0.57[a]	0.54[a]	0.718	0.65	1.63
Conn. Dens.	0.44	0.47[a]	39.889	1.05	3.19
Tb.Th	0.52[a]	0.66[a]	0.348	0.66	2.29
Tb.Sp	0.55[a]	0.64[a]	0.774	0.82	2.53
Fractal dimension	0.68[a]	0.61[a]	1.071	0.85	2.11
Plateness					
SMI	0.37	0.55[a]	0.540	0.75	2.63
Positive SMI	0.44	0.47[a]	0.815	0.71	1.84
Negative SMI	0.68[a]	0.76[a]	1.091	0.61	1.68
ev2/ev1	−0.12	−0.17	1.160	2.10	5.54
ev3/ev1	0.05	0.10	1.049	1.00	2.81

μCT, micro-CT; BS, bone surface; BS/TV, bone surface per total volume; BV/TV, bone volume per total volume; Conn. Dens., connectivity density; ev1/ev2/ev3, eigenvalues for longest/middle/shortest axis; Max, maximum; *R*, correlation coefficient, SD, standard deviation; SMI, structure model index; Tb.Sp, trabecular spacing; Tb.Th, trabecular thickness.
[a]Significant correlation ($p < 0.05$).

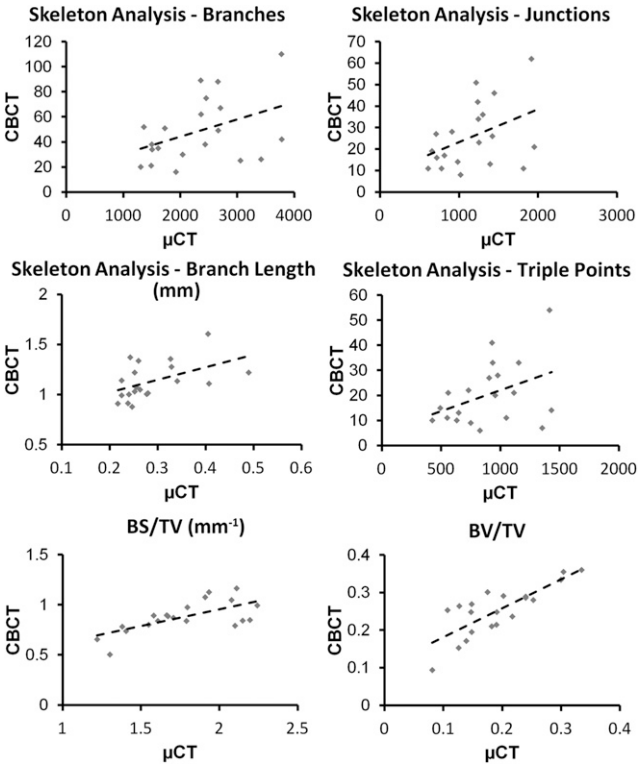

Figure 4 Scatter plots with linear fit (dashed line) for skeleton analysis and bone surface per total volume (BS/TV) and bone volume per total volume (BV/TV) bone parameters. *x*- and *y*-axis scales were adapted to the data distribution. μCT, micro-CT.

2 for BS/TV. Considerable overestimation was found for branch length and Tb.Th. For other parameters, calibration coefficients were between 0.54 and 1.16. Paired *t*-tests and Wilcoxon signed rank tests showed highly significant ($p < 0.001$) differences for all parameters, including those for which the calibration coefficient was close to 1.

Error after calibration

The error after calibration, that is the average of the difference between recalibrated CBCT values and corresponding μCT values, divided by the standard deviation of the μCT values, is shown in Table 1. Lower values correspond to smaller errors. The smallest error was seen for BV/TV, followed by branch length, negative SMI, BS/TV, anisotropy and Tb.Th. Despite showing significant correlation, Tb.Sp and fractal dimension had a larger error than did SMI and positive did SMI, for which R_P was not significant, illustrating the effect of forcing the calibration lines through (0, 0). Errors of other parameters were equal or higher than the standard deviation of the μCT values (*i.e.* ≥ 1).

Discussion

In this study, the applicability of bone microarchitecture parameters on CBCT was assessed using μCT as a reference. Out of 16 evaluated bone parameters, 8 showed significant Pearson and Spearman correlation. However, from the scatter plots (Figures 4–6) and error values (Table 1), it was seen that there is considerable uncertainty regarding the stability of these parameters.

A number of previous studies have investigated the use of one or more of these parameters in CBCT. Fractal dimension, and its relation with bone architecture, has been investigated on *in vitro*, animal and clinical CBCT images.[23–26] Various other studies have measured morphometric and other parameters, correlating values from CBCT with those from μCT and dual-energy X-ray absorptiometry.[27–31] Correlation coefficients were typically interpreted as "high". However, when comparing the present results with previous studies, it is important to note that a correlation coefficient has limited value when evaluating the potential clinical applications of these bone parameters. The interpretation of a correlation coefficient is mostly subjective and open for interpretation. As seen in Table 1, all coefficients with a value of 0.64 or higher were statistically significant. However, there is a large gap between statistical and clinical significance. Secondly, a high correlation does not imply that the numerical values correspond between the two variables, and large differences between bone parameter values of CBCT and other modalities have been revealed.[27–31] As seen in Table 1, correlation coefficients could be reasonably high even if the values for CBCT were severely under- or overestimated (as shown by the calibration coefficients). In other words, even if a bone parameter is found to have a high correlation coefficient, the value obtained from CBCT images may be far off the true value. In addition, correlation coefficients derived from a "best fit" are often unrealistic, that is, do not intercept the *x*- and *y*-axes at or close to (0, 0), limiting the

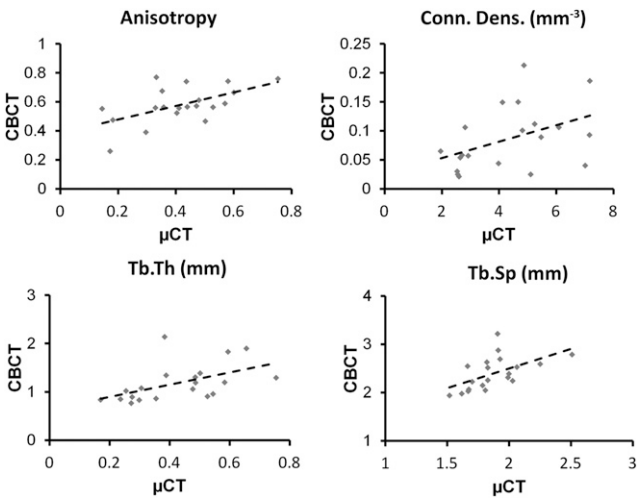

Figure 5 Scatter plots with linear fit (dashed line) for anisotropy, connectivity density (Conn. Dens.), trabecular thickness (Tb.Th) and trabecular spacing (Tb.Sp). *x*- and *y*-axis scales were adapted to the data distribution. μCT, micro-CT.

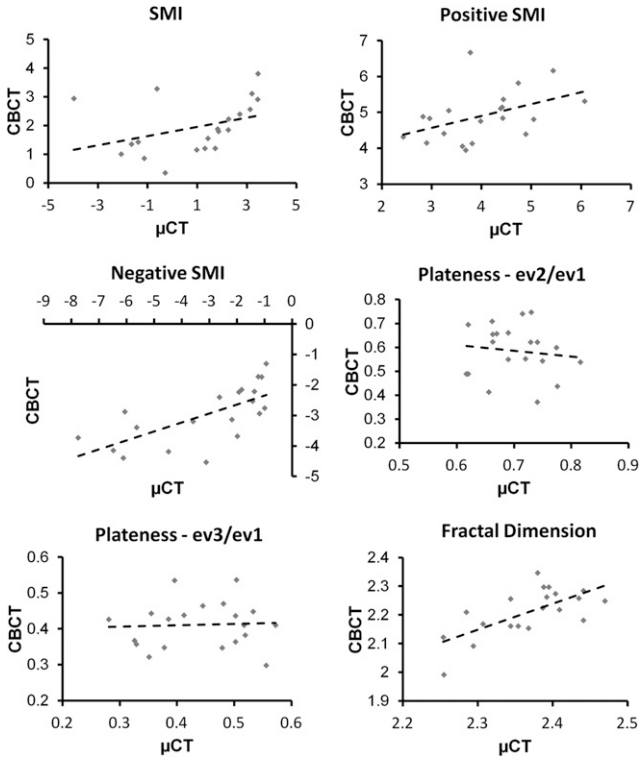

Figure 6 Scatter plots with linear fit (dashed line) for structure model index (SMI), plateness and fractal dimension. *x*- and *y*-axis scales were adapted to the data distribution. ev1/ev2/ev3, eigenvalues for the longest, middle and shortest axis of the trabeculae, respectively; μCT, micro-CT

clinical applicability of these regression lines. In our study, it is shown that after calibration using a regression line going through (0, 0) CBCT values can show notable errors even if the correlation coefficient was relatively high.

Another difference between the present study and previous research is the relatively large sample size ($n = 20$) in this study, which increases the reliability of the calculated correlation coefficients. Also, this study involved a small volume of interest, equal to the size of the extracted bone samples. When evaluating larger volumes, it may be possible to find a more consistent relationship between bone parameters from CBCT and μCT, but clinical applicability of such results are limited as bone evaluation prior to implant surgery will be limited to small volumes at a potential implant site.

To apply these bone parameters on clinical CBCT images, error margins should be as low as possible to get an accurate assessment of the patient's bone architecture. As even the highest correlation coefficient in our study (*i.e.* 0.80) shows large deviations from the regression line when looking at the scatter plot, it can be judged that a very high correlation may be required to consider the error margin as acceptable, although an exact cut-off between an acceptable and unacceptable correlation cannot be made at this point. *In vitro* and clinical studies, possibly retrospective, on the relationship between these bone parameters and implant stability and outcome may aid in the determination of new classification systems. However, before the step to clinical practice is made, further validation on the reliability of these parameters on CBCT data is needed. A bone parameter can only be applied clinically if its values are stable between different CBCT devices, although device-specific bone classifications are not entirely unfeasible. The values should also be independent of exposure parameters such as kVp, mAs and voxel size. It can be expected that values for each bone parameter will be different if the spatial resolution of the image varies, but the stability of each parameter for these variations remains to be found out. Two studies by Ibrahim et al[32,33] have investigated the effect of object location and scan parameters, showing varying stability. More evidence is needed to verify the nature of this instability and the possibility for defining correction factors (*e.g.* as a function of voxel size) to normalize values obtained from images obtained with different exposure settings.

The present study has a few limitations related to its translation to a clinical situation. First of all, it involved the scanning of small bone samples, with no simulation of soft tissue or jawbones. When using clinical exposure parameters, this may lead to an overestimation of image quality; however, in this study, the mAs was lower than that used for adult patients, which compensates for the lack of soft- and hard-tissue simulation. A second limitation that is applicable to all non-clinical studies is that the sample was stationary. As CBCT acquisitions are relatively slow (*i.e.* typically 10–40 s, 31 s in this study), movement of patients will always induce image blurring, even for very slight motion. It should therefore be kept in mind that image quality on clinical scans will be somewhat worse than that obtained during non-clinical experiments. A final limitation is that this study involved a single CBCT model. It has been shown that there is a large variability in spatial and contrast resolution between CBCTs, with the currently used model found at the high end of the image quality range.[10] Therefore, no conclusions can be made regarding CBCT as a whole; as mentioned above, differences between CBCTs as a result of varying exposure and reconstruction factors should be further investigated.

In conclusion, despite the overall correlation, this study demonstrates the large uncertainty associated with using bone microarchitecture parameters on CBCT images. Although clinically relevant parameter ranges are not available, the errors found in this study may be too high for most parameters to be considered for clinical application. Further evidence on the stability of these parameters in varying exposure conditions is warranted.

References

1. Adell R, Lekholm U, Rockler B, Brånemark PI. A 15-year study of osseointegrated implants in the treatment of the edentulous jaw. *Int J Oral Surg* 1981; **10**: 387–416.
2. Engquist B, Bergendal T, Kallus T, Linden U. A retrospective multicenter evaluation of osseointegrated implants supporting overdentures. *Int J Oral Maxillofac Implants* 1988; **3**: 129–34.
3. Jaffin RA, Berman CL. The excessive loss of branemark fixtures in type IV bone: a 5-year analysis. *J Periodontol* 1991; **62**: 2–4.
4. Drago CJ. Rates of osseointegration of dental implants with regard to anatomical location. *J Prosthodont* 1992; **1**: 29–31.
5. Jemt T, Lekholm U. Oral implant treatment in posterior partially edentulous jaws: a 5-year follow-up report. *Int J Oral Maxillofac Implants* 1993; **8**: 635–40.
6. Wirth AJ, Goldhahn J, Flaig C, Arbenz P, Müller R, van Lenthe GH. Implant stability is affected by local bone microstructural quality. *Bone* 2011; **49**: 473–8. doi: 10.1016/j.bone.2011.05.001
7. González-García R, Monje F. Is micro-computed tomography reliable to determine the microstructure of the maxillary alveolar bone? *Clin Oral Implants Res* 2013; **24**: 730–7. doi: 10.1111/j.1600-0501.2012.02478.x
8. Müller R, Van Campenhout H, Van Damme B, Van Der Perre G, Dequeker J, Hildebrand T, et al. Morphometric analysis of human bone biopsies: a quantitative structural comparison of histological sections and micro-computed tomography. *Bone* 1998; **23**: 59–66.
9. Swain MV, Xue J. State of the art of micro-CT applications in dental research. *Int J Oral Sci* 2009; **1**: 177–88. doi: 10.4248/IJOS09031
10. Pauwels R, Beinsberger J, Stamatakis H, Tsiklakis K, Walker A, Bosmans H, et al; SEDENTEXCT Project Consortium. Comparison of spatial and contrast resolution for cone-beam computed tomography scanners. *Oral Surg Oral Med Oral Pathol Oral Radiol* 2012; **114**: 127–35.
11. Tsai WH, Yu SS. Moment-preserving thresholding: a new approach. *Comput Vis Graph* 1985; **29**: 377–93.
12. Doube M, Klosowski MM, Arganda-Carreras I, Cordelières FP, Dougherty RP, Jackson JS, et al. BoneJ: free and extensible bone image analysis in ImageJ. *Bone* 2010; **47**: 1076–9. doi: 10.1016/j.bone.2010.08.023
13. Lorensen WE, Cline HE. Marching cubes: a high resolution 3D surface construction algorithm. Proceedings of the 14th Annual Conference on Computer Graphics and Interactive Techniques. July 1987; Association for Computing Machinery; 1987; pp. 163–9.
14. Fazzalari NL, Parkinson IH. Fractal dimension and architecture of trabecular bone. *J Pathol* 1996; **178**: 100–5.
15. Odgaard A, Gundersen HJ. Quantification of connectivity in cancellous bone, with special emphasis on 3-D reconstructions. *Bone* 1993; **14**: 173–82.
16. Toriwaki J, Yonekura T. Euler number and connectivity indexes of a three dimensional digital picture. *Forma* 2002; **17**: 183–209.
17. Odgaard A. Three-dimensional methods for quantification of cancellous bone architecture. *Bone* 1997; **20**: 315–28.
18. Harrigan TP, Mann RW. Characterization of microstructural anisotropy in orthotropic materials using a second rank tensor. *J Mater Sci* 1984; **19**: 761–7.
19. Dougherty RP, Kunzelmann K-H. Computing local thickness of 3D structures with ImageJ. *Microsc Microanal* 2007; **13**: 1678–9.
20. Hildebrand T, Rüegsegger P. A new method for the model-independent assessment of thickness in three-dimensional images. *J Microsc* 1997; **185**: 67–75.
21. Hildebrand T, Rüegsegger P. Quantification of bone microarchitecture with the structure model index. *Comput Methods Biomech Biomed Engin* 1997; **1**: 15–23.
22. Arganda-Carreras I, Fernández-González R, Muñoz-Barrutia A, Ortiz-De-Solorzano C. 3D reconstruction of histological sections: application to mammary gland tissue. *Microsc Res Tech* 2010; **73**: 1019–29. doi: 10.1002/jemt.20829
23. Hua Y, Nackaerts O, Duyck J, Maes F, Jacobs R. Bone quality assessment based on cone beam computed tomography imaging. *Clin Oral Implants Res* 2009; **20**: 767–71. doi: 10.1111/j.1600-0501.2008.01677.x
24. González-Martín O, Lee EA, Veltri M. CBCT fractal dimension changes at the apex of immediate implants placed using undersized drilling. *Clin Oral Implants Res* 2012; **23**: 954–7. doi: 10.1111/j.1600-0501.2011.02246.x
25. Huang Y, Van Dessel J, Liang X, Depypere M, Zhong W, Ma G, et al. Effects of immediate and delayed loading on peri-implant trabecular structures: a cone beam CT evaluation. *Clin Implant Dent Relat Res* 2014; **16**: 873–83. doi: 10.1111/cid.12063
26. Torres SR, Chen CS, Leroux BG, Lee PP, Hollender LG, Schubert MM. Fractal dimension evaluation of cone beam computed tomography in patients with bisphosphonate-associated osteonecrosis. *Dentomaxillofac Radiol* 2011; **40**: 501–5. doi: 10.1259/dmfr/14636637
27. Van Dessel J, Huang Y, Depypere M, Rubira-Bullen I, Maes F, Jacobs R. A comparative evaluation of cone beam CT and micro-CT on trabecular bone structures in the human mandible. *Dentomaxillofac Radiol* 2013; **42**: 20130145. doi: 10.1259/dmfr.20130145
28. Hsu JT, Wang SP, Huang HL, Chen YJ, Wu J, Tsai MT. The assessment of trabecular bone parameters and cortical bone strength: a comparison of micro-CT and dental cone-beam CT. *J Biomech* 2013; **46**: 2611–18. doi: 10.1016/j.jbiomech.2013.08.004
29. Parsa A, Ibrahim N, Hassan B, van der Stelt P, Wismeijer D. Bone quality evaluation at dental implant site using multislice CT, micro-CT, and cone beam CT. *Clin Oral Implants Res* 2015; **26**: e1–7. doi: 10.1111/clr.12315
30. Ibrahim N, Parsa A, Hassan B, van der Stelt P, Aartman IH, Wismeijer D. Accuracy of trabecular bone microstructural measurement at planned dental implant sites using cone-beam CT datasets. *Clin Oral Implants Res* 2014; **25**: 941–5. doi: 10.1111/clr.12163
31. Ho JT, Wu J, Huang HL, Chen MY, Fuh LJ, Hsu JT. Trabecular bone structural parameters evaluated using dental cone-beam computed tomography: cellular synthetic bones. *Biomed Eng Online* 2013; **12**: 115. doi: 10.1186/1475-925X-12-115
32. Ibrahim N, Parsa A, Hassan B, van der Stelt P, Aartman IH, Wismeijer D. The effect of scan parameters on cone beam CT trabecular bone microstructural measurements of human mandible. *Dentomaxillofac Radiol* 2013; **42**: 20130206.
33. Ibrahim N, Parsa A, Hassan B, van der Stelt P, Aartman IH, Nambiar P. Influence of object location in different FOVs on trabecular bone microstructure measurements of human mandible: a cone beam CT study. *Dentomaxillofac Radiol* 2014; **43**: 20130329. doi: 10.1259/dmfr.20130329